Amorphization in α-boron: A molecular dynamics study

Pavel A. Pokatashkin,* Pavel Yu. Korotaev, and Alexei V. Yanilkin
Dukhov Research Institute of Automatics (VNIIA), 22 Sushchevskaya, Moscow 127055, Russia
(Received 30 November 2016; revised manuscript received 10 February 2017; published 28 February 2017)

Thin amorphous bands are often thought to be the cause of drastic change of properties in boron-based ceramics. We investigate possible mechanisms of amorphization by performing a large-scale molecular dynamics study of defect formation in α-boron. Activation of the [101]/(010) slipping system leads to the nanotwin formation. We found no evidence that the nanotwin can become amorphous; it remains stable at high pressures and temperatures. However, inherent plastic deformation leads to local increasing of density that is the precursor of so-called amorphization.

DOI: 10.1103/PhysRevB.95.064113

I. INTRODUCTION

Boron (B) is a unique element of amazing complexity. Pure boron is comparatively rarely used and poorly studied due to the difficulties of its preparation and high chemical activity. Unlike the elemental material, B-rich compounds are of great importance [1]. They find applications in engineering, military, nuclear, and electronics industries due to their distinctive combinations of properties, e.g., superhardness, low density, high melting temperature, thermal and chemical stability, etc.

The phase diagram of B is still discussed [2–4]. We can mention α- and β-rhombohedral, tetragonal, γ-phases, and structure similar to α-gallium. The most studied polymorph is the one with simplest structure, α-rhombohedral phase. It is the most stable allotrope in a wide region of the P-T diagram: from ambient conditions up to pressures of $\sim$20 GPa and temperatures $\sim$1400 K. Furthermore, the structure of α-B is the parent [1] to many boron-rich materials (BRM). It can be described as a 12-atom icosahedra placed at the vertices of a rhombohedral lattice. There are two nonequivalent crystallographic sites at this configuration: Six atoms in the icosahedron have bonds with nearby icosahedra, while six others have not. Atoms at those sites are called polar and equatorial respectively. With the addition of a linear three- or two-atom chain, placed along the main diagonal of a rhombohedron, structures of boron carbide ($B_{12}C_3$), boron suboxide ($B_{12}O_2$), boron subphosphide ($B_{12}P_2$), boron subnitride ($B_{13}N_2$), boron subarsenide ($B_{12}As_2$), etc., could be obtained. We should also mention that such peculiar structure provides wide opportunities of doping BRM with foreign atoms. Various theoretical and experimental research studies have been performed to study changes in mechanical and electronic properties of doped materials [5–10].

Active usage of various boron ceramics underlines the importance of α-B modeling: With similar unique structure and mechanical properties, one can assume that, e.g., key patterns of crystallographic defects would also be similar. The structure of α-B and discussed BRM have trigonal symmetry ($R\bar{3}m$ space group). Thus both rhombohedral and hexagonal representations could be used. In order to avoid ambiguity, rhombohedral representation is used throughout the paper except where otherwise noted. It is more clear because the origin is placed at the center of the icosahedron and the axis directions coincide with the bonds, connecting polar atoms of nearby icosahedra.

Let us discuss defects in α-boron and BRM, boron carbide and boron suboxide in particular. As processed, boron carbide has a large number of twins but no dislocations [11]. Twinning along the {100} planes is observed in boron suboxide [12]. Dislocations with $b = \langle 110\rangle$ gliding at {111} plane are observed at deformed boron carbide. Edge dislocations with $b = \langle 110\rangle$ Burgers vector and $g = \langle \bar{1}10\rangle$ line direction are found in boron subarsenide [13].

The main issue of the work is to shed light on the formation mechanism of thin amorphous zones' peculiar defect, that is observed in BRM. It is found in various types of experiments, including ballistic impact [14], nanoindentation [15–18], and depressurization from high pressures [19]. Those bands could be roughly parallel to several families of crystallographic planes: {210} [14,17], {100} [15,16], {110} [18], {111} [17], {310} [19], and {$\bar{1}$11} [20]. Formation of a peculiar deformation defect, thin amorphous bands, is often thought to be the cause of drastic change of properties in boron-based ceramics [14], e.g., reducing of ballistic shielding performance and loss of hardness.

Let us discuss what the conditions are when amorphous zones are formed. First of all it should be mentioned that amorphous bands can be found only in experiments where high loading was applied. In ballistic impact experiments, Chen [14] observed abrupt decrease of shielding properties of boron carbide at high velocity impact. It was estimated that critical velocities correspond to pressures of $\sim$22−23 GPa. At high-velocity impact (>900 m/s) a large number of small fragments due to extensive cleavage was observed. High-resolution electron microscopy (HREM) shows that amorphous zones are present in those fragments. While at subcritical velocity impact only twins and stacking faults in the (010) plane were observed. Yan [19] performed *in situ* high-pressure Raman spectroscopy during loading and unloading of boron carbide in diamond anvil cell. It was found that Raman peaks corresponding to amorphous bands begin to appear only during the unloading stage at pressures of $\sim$16 GPa if the maximal loading pressure exceeded the critical value of $\sim$25 GPa. Recently an experimental paper by Zhao [20] was published, who performed laser shock compression of boron carbide. At a shock stress of $\sim$50 GPa amorphous bands were observed.

*p.a.pokatashkin@gmail.com

At lower compression of ∼25 GPa only planar faults were seen.

It should be noted that the exact mechanism of the amorphous band formation is still debated. Reddy *et al.* showed evidence of shear-induced amorphization in boron carbide and suboxide [15,16] during nanoindentation. Mechanism of shear-induced amorphization along the (001) plane was proposed.

Experimental observations [21] show that there are no structural transitions in boron carbide up to pressures of ∼40 GPa. *Ab initio* modeling [22] shows that there are no structural transitions in single crystal of B_4C up to quasihydrostatic pressures of 60 GPa. The crucial role of nonhydrostatic stress on the process of amorphization in boron carbide was shown both experimentally [19] and by *ab initio* modeling [23].

Atomistic modeling is widely used in studying the properties of crystallographic defects. Unfortunately some peculiar phenomena, e.g., the above-mentioned amorphous bands, are too large to be studied by *ab initio* approaches due to the computational complexity. That is why use of classical molecular dynamics (MD) could provide useful information on the processes that lead to formation of these zones and their properties. Shear-induced amorphization in defect-free boron carbide was studied [24] by means of force-field MD but very high shear stresses were obtained. That is why study of possible reasons of amorphous bands formation should be continued.

The key idea of the present work is investigating the mechanism of amorphous zone formation. Planar defects can influence this process in two possible ways. First of all, a planar defect can become amorphous under pressure due to the defect structure. Second, the process of planar defect formation can be accompanied by amorphization. We focus on MD modeling of α-B to study the key patterns of amorphization mechanism that would be similar in BRM.

The accuracy of results obtained by MD modeling are governed by the quality of the interatomic potential. Precision of a potential for one chemical element is often better comparing to the potentials for binary or ternary systems. Hence, modeling of α-B could provide useful insights on key patterns of amorphization in BRM. We use the angular-dependent potential [25] for α-boron [26]. It was obtained by force-matching method [27] and trained in a wide pressure and temperature range.

The paper is organized as follows. Static calculations are performed to study the properties of possible planar defects. They are discussed in Sec. II. Large-scale MD simulations are performed to study dynamic formation of planar defects and amorphization. Details are given in Sec. III. The conclusions are made in Sec. IV.

II. STATIC CALCULATIONS

A. Modified γ-surface of the (010) plane

Since introducing by Vitek in 1968, the γ-surface [28] is used as a powerful tool for studying slip deformation. Let us note the key idea: introducing $\gamma = E - E_{00}$, where E_{00} is the energy of perfect lattice and E is the energy, when one half of a crystal is displaced along the gliding plane. Thus, the γ-surface is obtained as a function of slipping direction values (let it be x and z). Local maxima and minima on this surface represent unstable and stable stacking faults, giving information about preferable transition paths, Peierls barriers, etc.

Since α-boron has peculiar structure, e.g., acting as a molecular crystal during compression [26], energy minimization after sliding should be performed. The importance of atomic relaxation was shown at similar calculations of γ-surfaces for such molecular crystals as cyclotrimethylene trinitramine (RDX) [29], triaminotrinitrobenzene (TATB) [30], or Mg_2SiO_4 [31]. In order to emphasize that energy is obtained after minimization is performed, we shall call the obtained surface the modified γ-surface.

Let us briefly summarize the computational details. All simulations are performed with the LAMMPS code [32]. Visualizations are made by the ATOMEYE package [33]. The potential for α-B is described in previous work [26].

Studying of the modified γ-surface is performed in a triclinic simulation box. Periodic boundary conditions (PBC) are imposed. Here the x, y, z axes are parallel to $[\bar{1}01]$, $[0\bar{1}1]$, [001] directions respectively. Thus the (xz) plane is the (010) plane $[(\bar{1}101)_h$ in hexagonal representation], where amorphous zones are observed [15,16]. This plane is shown in Fig. 1 (upper panel). Here and throughout the paper atoms are colored for visual perception purposes only. The importance of the [101] direction will be shown later.

Calculation scheme is presented in Fig. 1 (lower panel). One half of the crystal was displaced along the (010) plane. A slice of 2 icosahedra in height (in the y direction) was deleted; thus distance between free surfaces is greater than the potential cutoff radius. Slices of 1 icosahedra in height (along the y direction) on both sides of free surfaces were frozen to simulate the innermost layers of a bulk. They are not allowed to move either at energy minimization or at molecular dynamics simulations (discussed below).

The simulated region should be large enough to let the gliding plane be far away from its periodic images. We have found that the $6 \times 30 \times 6$ supercell is sufficient to neglect the effects of periodicity and free surfaces. Consequently, the simulated system has the form of a stretched parallelepiped and contains 12 096 atoms.

We calculated the modified γ surface on a 50×50 mesh. Let us discuss the key patterns of the result presented in Fig. 2. One could note that almost entire surface can be divided at two regions: with high ($>1.0\,J/m^2$) and low ($<0.2\,J/m^2$) energies. Significant difference between structures at these regions may be assumed. Indeed, the high surface energy region stands for general stacking fault. Two different structural changes were observed at the other area. The first one is the relaxation of the displacement defect into a single crystal, with increasing of shear stress components. Second option observed is relaxation into nanotwinned structure.

B. Nanotwinning

Let us discuss the structure in local minima at the point (0.7, 0.6) shown in Fig. 3. Nanotwinning (NT) is observed. It should be mentioned that this phenomena occurs in boron and BRM; e.g., the new structure of boron with C_{mcm} space

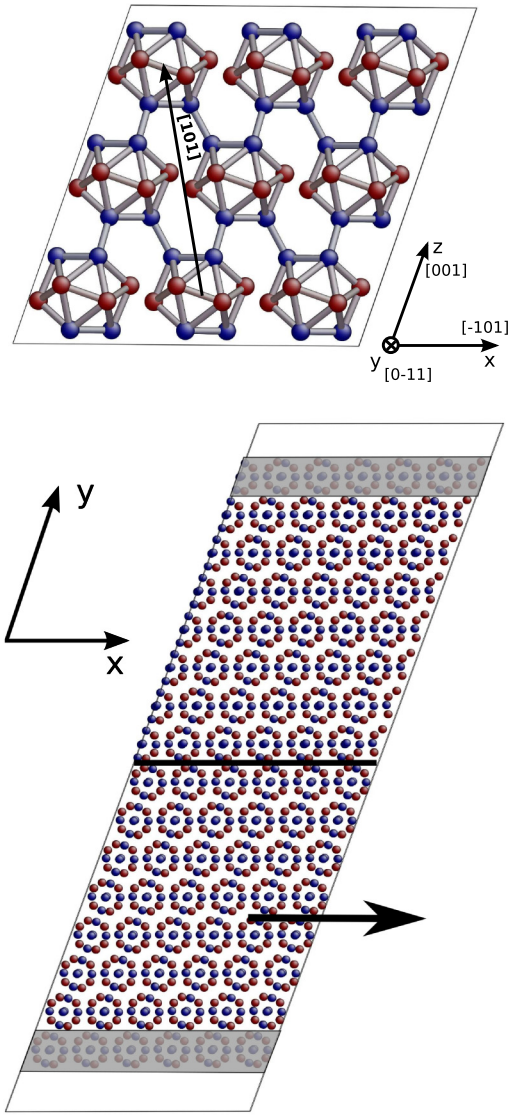

FIG. 1. (Upper panel) The (010) plane. Blue circles are boron atoms in the polar sites, and red circles are boron atoms in the equatorial sites. The [101] direction is shown by the black arrow. (Lower panel) The simulation box used in γ-surface calculations. Gray-shaded areas show regions of "frozen" atoms, and parts of the crystal are divided by solid black line.

group was predicted by Pickard [34]. It can be viewed as a nanotwinned α-B and is slightly higher ($\sim$10 meV/atom) in enthalpy [35]. Later, An *et al.* [36] showed both theoretically and experimentally that the NT boron suboxide is the most stable structure.

In our calculations, the surface energy of the NT is $-34\,\mathrm{mJ/m^2}$. The result is in reasonable agreement with other calculations. Now let us discuss stability of the NT defect at high pressures and temperatures.

Considering such peculiar structure of α-B, one must take into account that key patterns of the modified γ-surface might be different at high pressures. We perform similar calculations of the modified γ-surface with the bulk crystal initially corresponding to pressures of 10, 20, 30, and 40 GPa. This evolution is shown in Fig. 4. One can notice that key

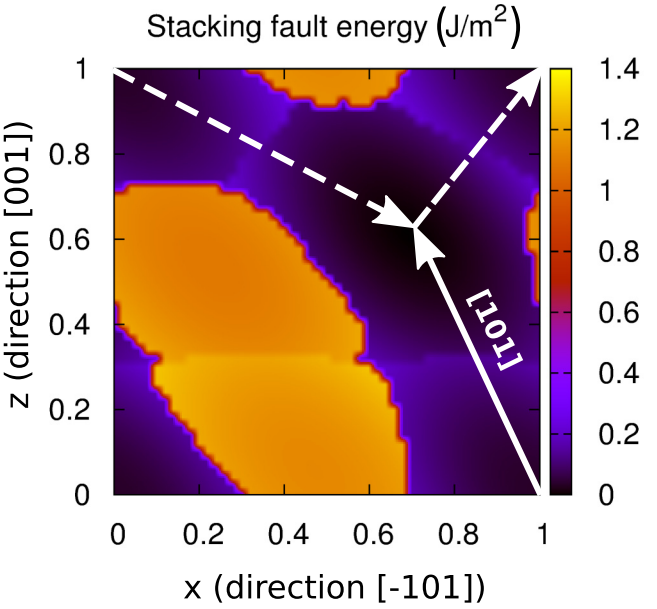

FIG. 2. Projection of the (010) plane modified γ-surface. Probable preferable partial Burgers vectors are shown by dashed arrows. The activated slipping system is shown by the solid arrow.

patterns are the same. The local minima and maxima do not move, though the barriers have changed.

We have also studied thermal stability of the NT. The simulation details are as follows: First the NT is obtained and energy minimization is performed. Then simulations in the NVE ensemble at several given temperatures for several nanoseconds are performed. Our results show that the NT defect is as stable as the bulk crystal till melting at $\sim$1600 K occurs. We should also note that melting starts in the bulk, not in the NT. Thus we can conclude that the NT shall be

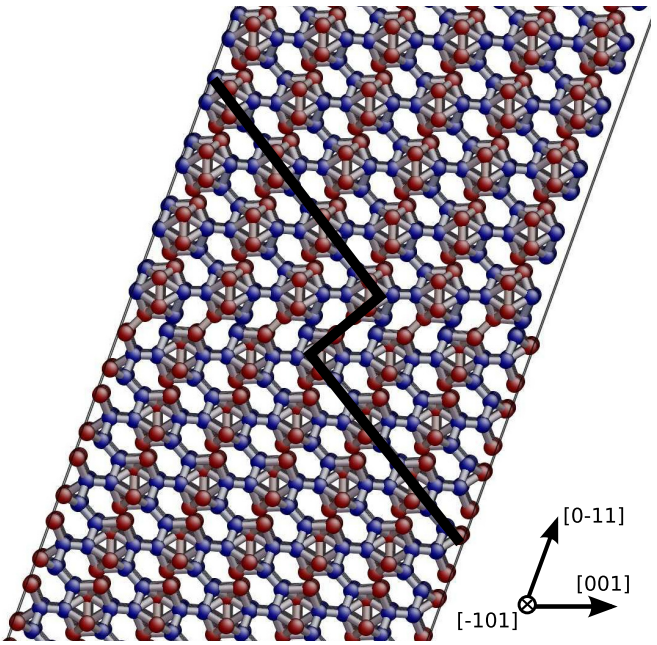

FIG. 3. Nanotwinned structure at the (0.7, 0.6) point. Solid black line is a guide to the eye.

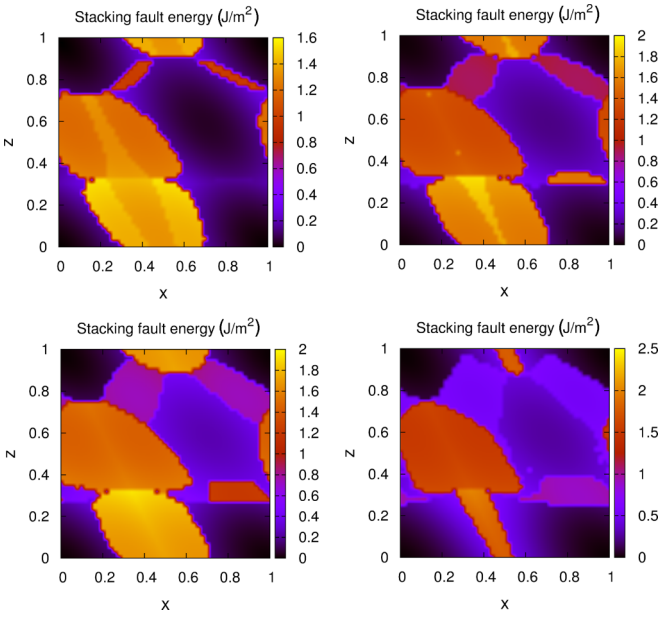

FIG. 4. Projection of the (010) plane modified γ-surface. Initial pressures of 10 (left upper panel), 20 (right upper panel), 30 (left lower panel), and 40 (right lower panel) GPa are present.

considered stable in a wide pressure and temperature range. No evidence that the discussed NT can become amorphous.

III. DYNAMIC SIMULATIONS

A. Linear defects

The most similar case to the process of shock waves propagation is uniaxial loading. Thus we are studying if the discussed NT could be formed during uniaxial loading.

The simulation details are as follows. We considered an orthogonal stretched simulation box ($59 \times 68 \times 188$ Å). The z axis is parallel to the [111] direction. PBC are used. A spherical hole (7 Å radius) is introduced in the center to ease the formation of defects. Thus, total number of atoms in the simulation box is ∼100 000. All dynamic simulations are performed with a constant time step of 1 fs.

We considered compression along the [111] direction at constant engineering strain rate. In simulations with strain rate 8×10^8 s^{-1}, imposed for 0.2 ns, shear deformation was observed. At this type of simulation, pressure gradually rises, until the critical condition is achieved and plastic deformation occurs. That leads to abrupt dropping of pressure due to the formation of defects. The stress-strain relation is presented in Fig. 5. Before the stress relaxation due to plastic deformation took place, stress tensor components were $\sigma_{xx} \approx \sigma_{yy} = 14$ GPa and $\sigma_{zz} = 51$ GPa (that corresponds to pressure of 26 GPa).

Simulations with an induced void are justifiable because boron and BNM often have porosity. Still, studying how such specific defects influence the material properties is necessary. We perform several similar calculations and vary

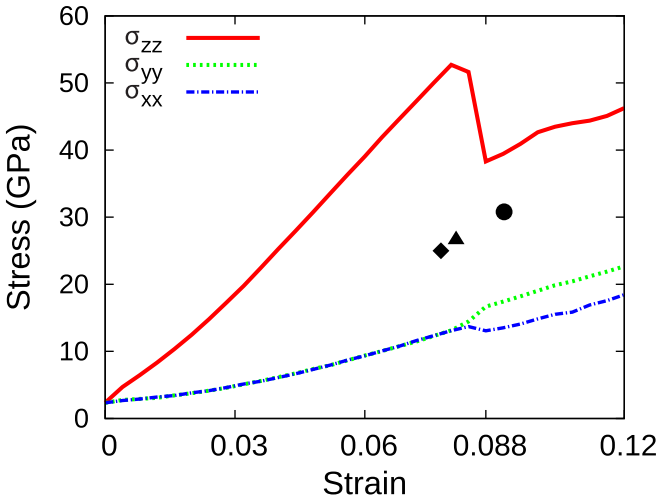

FIG. 5. Stress-strain relation. At $\epsilon = 0.088$ plastic deformation occurred. Filled symbols stand for critical pressures at calculations with hole radius of 4 Å (circle), 7 Å (triangle), and 10 Å (diamond).

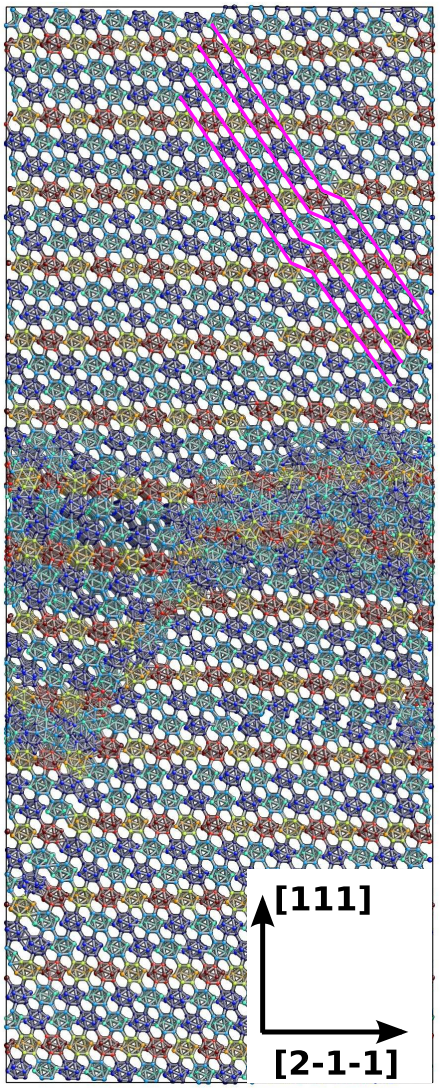

FIG. 6. Snapshot at strain $\epsilon = 0.088$. Atoms are colored for the convenience of visual perception only. Pink lines show the [101]/(010) shear displacement.

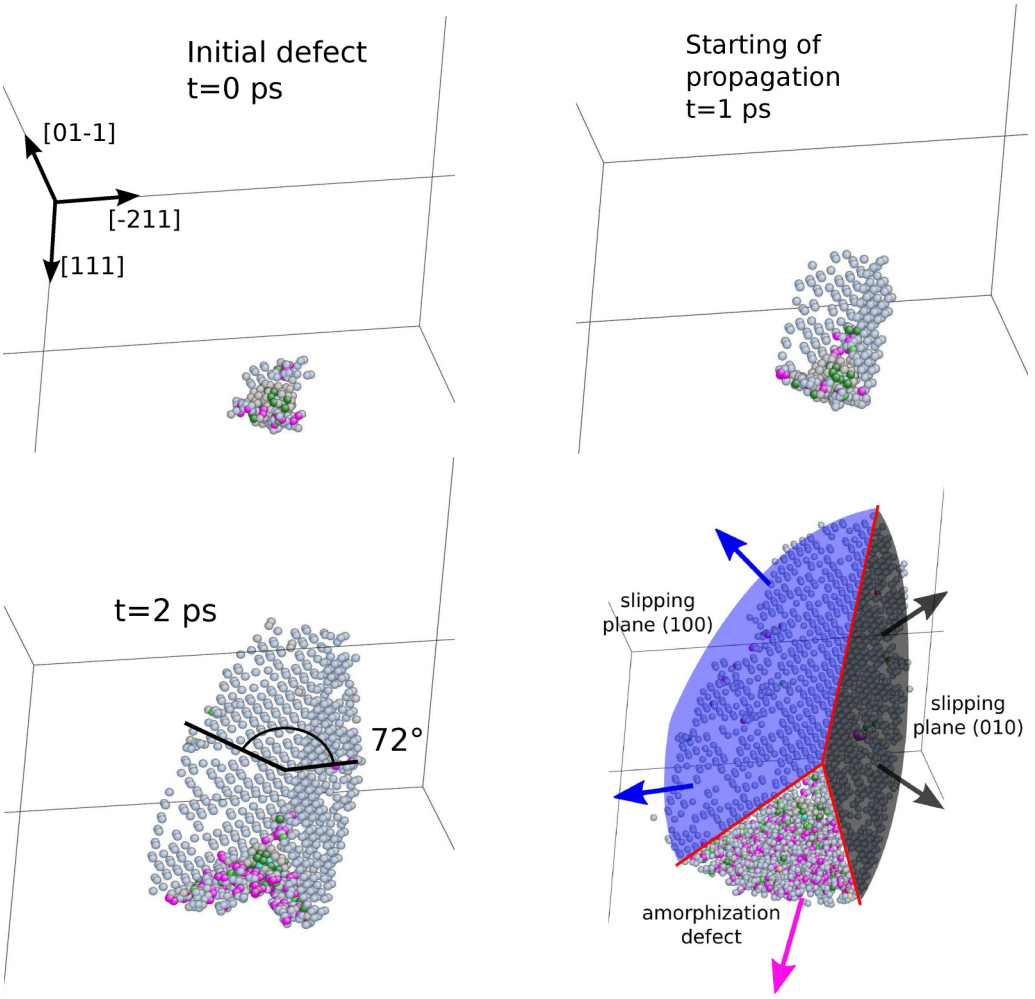

FIG. 7. Atomistic configurations, showing the propagation of the amorphization defect. Only atoms with coordination number bigger than the matrix are shown. Time step between snapshots is 1 ps.

the radius of a hole. We observe critical stresses to be lower in simulations with larger voids. In Fig. 5 critical pressures in simulations with 4 Å, 7 Å, and 10 Å holes are also shown. Those stand for 42, 198, and 558 deleted atoms. This result is reasonable, because a larger void induces larger distortions to the crystal structure, allowing plastic deformation to occur more easily. Nevertheless, the qualitative mechanism of deformation remains the same.

We observe the slipping system $\langle 101\rangle/\{010\}$ to be activated. Atomic configuration at strain $\epsilon = 0.088$ is presented in Fig. 6. That is just the same result as in shock waves simulation [26]. This result is in agreement with the observation of the formation of stacking faults and twins in the (100) plane during ballistic impact at subcritical velocities by Chen [14].

B. Amorphization

Let us analyze the proposition [15,16] that shear along the (010) plane is the defect leading to amorphization in boron carbide and suboxide. In the present work, we found that the preferable (010)/[101] slipping system is activated at uniaxial loading, it was activated at simulations of high-velocity impact [26]. Nevertheless, there is no evidence that the discussed shear defect would be unstable. It has very low formation energy in the case of α-B; it is even the ground state in the case of boron suboxide, and because as-sintered boron carbide has a lot of such twins [37–41] we can assume that the formation energy in this case is quite low too. It is stable up to very high temperatures and pressures. The aforesaid reasons close the opportunity of activating the (010)/[101] slipping system as the precursor of cleavage. Nevertheless, it is observed. Hereafter we present our view on this enigma.

Neither at present calculations nor at shock waves simulations [26] have we found the discussed slipping system to be activated alone. It is always accompanied by another displacement defect originating from one place. If amorphization takes place in the latter, then studying the tip of the amorphous band would reveal shear displacement along the (010) plane. This proposition is in agreement with the most recent results by An [18]: The twin boundary and the tip of amorphous zone are originating from one place in boron suboxide after nanoindentation. The difference between our results is that the amorphous zone was found to lay in the (011) plane in the discussed paper, while we cannot distinguish the amorphization plane. In a recent paper by Subhash [42] a similar result is obtained: Amorphous zone

and crystallographic defects (dislocations, lattice rotation) are observed contiguously.

Using the PBC allows deformation defects to reflect through boundaries, making study of their properties more complicated. Thus we perform similar calculations with the system, expanded in x and y directions. A lower strain rate of 10^8 s^{-1} is considered. Therefore, total simulation time increased to 2 ns. The new simulation box ($177 \times 187 \times 188$ Å) has total number of atoms of ~0.86 M.

Crystallographic defects change local coordination structure. That is why focusing our view on atoms with distinctive coordination numbers (CN) allows tracking the defect propagation in a more convenient way. Atomistic configurations showing defect activation and propagation are shown in Fig. 7. Atoms with CN bigger (and lower but the latter are nearly unseen) than the rest of the matrix are only visible. As is shown in Fig. 7 (lower right panel) three regions could be distinguished. Two planar faults (marked by gray and blue regions) consist mostly of gray atoms. Another so-called amorphization defect contains gray(CN = 8, cutoff radii 2.02 Å), purple (CN = 9), and green (CN = 10) atoms. Those planar faults stands for the border of the shear displacement activated by the (010)/[101] slipping system. Colored arrows show direction of defects propagation. The dihedral angle between those faults is ~72° which is in agreement with the theoretical predictions of the angle between {010} crystallographic planes [18].

The biplanar shear displacement results in local increasing of density at the amorphization defect, motivating its propagation. However, we cannot distinguish the preferable direction of propagation. Moreover, in some simulations the amorphization defects definitely have propagated at different directions, even changing the direction line on the move. Very high sensitivity to local strain fields could be proposed. That might be the reason why such variety of amorphization planes has been found, as we discussed earlier.

IV. CONCLUSIONS

Formation and propagation of thin amorphous bands in BRM are still studied. We perform large-scale MD simulations to study the propositions that a planar defect is the precursor of forthcoming amorphization. The question is the following: What is the planar fault leading to amorphization? We found that the NT, activated by the (010)/[101] slipping system, shall stablize the crystallographic defect with pressure and temperature. Thus, the amorphization defect is not the shear displacement activated by the (010)/[101] slipping system. Nevertheless, this shear displacement induces local increase of density that motivates propagation of the so-called amorphization defect, which originates from one place. Unfortunately, the exact mechanism of its propagation and preferable directions are also unclear. That is because the direction of propagation could change on the move, due to sensitivity to the local strain fields. Perhaps it is the reason that at various experiments thin amorphous bands are found to lay in a large number of crystallographic planes. Furthermore, its properties could differ in various BRM.

[1] B. Albert and H. Hillebrecht, Angew. Chem. Int. Ed. **48**, 8640 (2009).

[2] M. A. White, A. B. Cerqueira, C. A. Whitman, M. B. Johnson, and T. Ogitsu, Angew. Chem. Int. Ed. **54**, 3626 (2015).

[3] A. R. Oganov, J. Chen, C. Gatti, Y. Ma, Y. Ma, C. W. Glass, Z. Liu, T. Yu, O. O. Kurakevych, and V. L. Solozhenko, Nature (London) **457**, 863 (2009).

[4] Q. An, K. M. Reddy, K. Y. Xie, K. J. Hemker, and W. A. Goddard, Phys. Rev. Lett. **117**, 085501 (2016).

[5] M. K. Kolel-Veetil, R. M. Gamache, N. Bernstein, R. Goswami, S. B. Qadri, K. P. Fears, J. B. Miller, E. R. Glaser, and T. M. Keller, J. Mater. Chem. C **3**, 11705 (2015).

[6] J. E. Proctor, V. Bhakhri, R. Hao, T. J. Prior, T. Scheler, E. Gregoryanz, M. Chhowalla, and F. Giulani, J. Phys. Condens. Matter **27**, 015401 (2015).

[7] W. Hayami and S. Otani, J. Phys. Chem. C **112**, 2711 (2008).

[8] T. Nagatochi, H. Hyodo, A. Sumiyoshi, K. Soga, Y. Sato, M. Terauchi, F. Esaka, and K. Kimura, Phys. Rev. B **83**, 184507 (2011).

[9] Q. An and W. A. Goddard, J. Phys. Chem. Lett. **5**, 4169 (2014).

[10] A. B. Rahane, V. Kumar, and J. S. Dunn, J. Am. Ceram. Soc. **98**, 2223 (2015).

[11] B. M. Moshtaghioun, D. G. García, and A. D. Rodríguez, Mater. Des. **88**, 287 (2015).

[12] H. Hubert, B. Devouard, L. A. Garvie, M. O'keeffe, P. R. Buseck, W. T. Petuskey, and P. F. McMillan, Nature (London) **391**, 376 (1998).

[13] C. E. Whiteley, Y. Zhang, A. Mayo, J. H. Edgar, Y. Gong, M. Kuball, and M. Dudley, in MRS Proc., Vol. 1307 (Cambridge University Press, Cambridge, UK, 2011), pp. mrsf10–1307.

[14] M. Chen, J. J. W. McCauley, and K. J. K. Hemker, Science **299**, 1563 (2003).

[15] K. Madhav Reddy, A. Hirata, P. Liu, T. Fujita, T. Goto, and M. W. Chen, Scr. Mater. **76**, 9 (2014).

[16] K. M. Reddy, P. Liu, A. Hirata, T. Fujita, and M. W. Chen, Nat. Commun. **4**, (2013).

[17] D. Ge, V. Domnich, T. Juliano, E. A. Stach, and Y. Gogotsi, Acta Mater. **52**, 3921 (2004).

[18] Q. An, K. M. Reddy, J. Qian, K. J. Hemker, M. W. Chen, and W. A. Goddard Iii, Nat. Commun. **7**, 11001 (2016).

[19] X. Q. Yan, Z. Tang, L. Zhang, J. J. Guo, C. Q. Jin, Y. Zhang, T. Goto, J. W. McCauley, and M. W. Chen, Phys. Rev. Lett. **102**, 075505 (2009).

[20] S. Zhao, B. Kad, B. A. Remington, J. C. LaSalvia, C. E. Wehrenberg, K. D. Behler, and M. A. Meyers, Proc. Natl. Acad. Sci. USA **113**, 12088 (2016).

[21] V. Domnich, S. Reynaud, R. A. Haber, and M. Chhowalla, J. Am. Ceram. Soc. **94**, 3605 (2011).

[22] P. Korotaev, P. Pokatashkin, and A. Yanilkin, Model. Simul. Mater. Sci. Eng. **24**, 015004 (2016).

[23] P. Korotaev, P. Pokatashkin, and A. Yanilkin, Comput. Mater. Sci. **121**, 106 (2016).

[24] Q. An and W. A. Goddard, Phys. Rev. Lett. **115**, 105501 (2015).

[25] Y. Mishin, Acta Mater. **53**, 4029 (2005).

[26] P. Pokatashkin, A. Kuksin, and A. Yanilkin, Model. Simul. Mater. Sci. Eng. **23**, 045014 (2015).
[27] F. Ercolessi and J. B. Adams, EPL **26**, 583 (1994).
[28] V. Vítek, Philos. Mag. **18**, 773 (1968).
[29] L. B. Munday, S. D. Solares, and P. W. Chung, Philos. Mag. **92**, 3036 (2012).
[30] N. Mathew and T. D. Sewell, Philos. Mag. **95**, 424 (2015).
[31] P. Carrez, P. Cordier, D. Mainprice, and A. Tommasi, Eur. J. Mineral. **18**, 149 (2006).
[32] S. Plimpton, J. Comput. Phys. **117**, 1 (1995).
[33] J. Li, Model. Simul. Mater. Sci. Eng. **11**, 173 (2003).
[34] C. J. Pickard and R. J. Needs, J. Phys. Condens. Matter **23**, 053201 (2011).
[35] C. He and J. X. Zhong, AIP Adv. **3**, 042138 (2013).
[36] Q. An, K. M. Reddy, H. Dong, M.-W. Chen, A. R. Oganov, and W. A. Goddard, Nano Lett. **16**, 4236 (2016).
[37] Y. Li, Y. Zhao, W. Liu, Z. Zhang, R. Vogt, E. Lavernia, and J. Schoenung, Philos. Mag. **90**, 783 (2010).
[38] T. Fujita, P. Guan, K. Madhav Reddy, A. Hirata, J. Guo, and M. Chen, Appl. Phys. Lett. **104**, 021907 (2014).
[39] B. Niu, F. Zhang, J. Zhang, W. Ji, W. Wang, and Z. Fu, Scr. Mater. **116**, 127 (2016).
[40] E. M. Heian, S. K. Khalsa, J. W. Lee, Z. A. Munir, T. Yamamoto, and M. Ohyanagi, J. Am. Ceram. Soc. **87**, 779 (2004).
[41] Z. Guan, B. Cao, Y. Yang, Y. Jiang, D. Li, and T. T. Xu, Nanoscale Res. Lett. **9**, 30 (2014).
[42] G. Subhash, A. P. Awasthi, C. Kunka, P. Jannotti, and M. DeVries, Scr. Mater. **123**, 158 (2016).